ChemComm

Accepted Manuscript

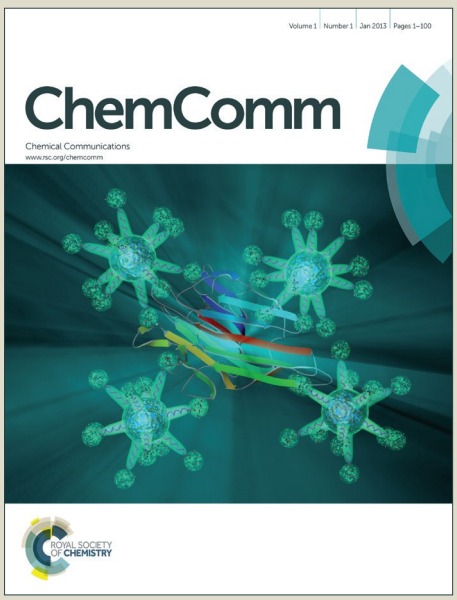

ROYAL SOCIETY OF CHEMISTRY

www.rsc.org/chemcomm

Journal Name

COMMUNICATION

Synthesis and Photocatalytic Activity of Porous Bismuth Oxychloride Hexagonal Prisms

Received 00th January 20xx,
Accepted 00th January 20xx

DOI: 10.1039/x0xx00000x

www.rsc.org/

Liyong Ding,[a] Huan Chen,[a] Qingqian Wang,[a] Tengfei Zhou,[b] Qingqing Jiang,[a] Yuhong Yuan,[a] Jinlin Li[a] and Juncheng Hu*[a]

Porous BiOCl hexagonal prisms have been successfully prepared through a simple solvothermal route. These novel BiOCl HPs with porous structures are assembled by nanoparticles and exhibit high activity and selectivity toward the photocatalytic aerobic oxidation of benzyl alcohol to benzaldehyde and degradation of methyl orange.

Bismuth oxyhalides are an important class of functional materials with interesting electronic, optical, magnetic, photocatalytic properties[1-5]. In recent years, notable efforts have been devoted to the development of nanostructured bismuth oxyhalides as photocatalysts for the decomposition of organic pollutants[6], fixation of N_2 to NH_3[7], oxidation of secondary amines to corresponding imines[8], and so on. As an important tetragonal matlockite structure, with a layer structure characterized by $[Bi_2O_2]^{2+}$ slabs interleaved by double slabs of halogen ions, up to date, numerous morphology of bismuth oxyhalides have been prepared, such as nanobelts[9-11], nanosheets[12-16], nanodiscs[17], and hierarchical structures assembled by nanosheets[18-21], as we know, nearly all the reported routes led to sheet-like bismuth oxyhalides. We have known that the physicochemical properties of materials are potently dependent on its structures, including the morphology, shape and size, as well as size distribution. Therefore, rational structural designment is indispensable for exploring the potential of bismuth oxyhalides as smart and functional materials, and one can boost or maximize the photocatalytic performances by structural design. Despite the recent significant progress in the preparation of bismuth oxyhalides, the rational design, fabrication and photocatalytic study of porous bismuth oxychloride hexagonal prisms have not been reported.

Herein, we demonstrate the controlled fabrication of porous BiOCl hexagonal prisms. To the best of our knowledge, this is the first report on engineering this unique porous BiOCl HPs. The surface and internal structures of the porous BiOCl HPs are fully characterized. These novel BiOCl HPs with porous structures exhibit high activity and selectivity toward the photocatalytic aerobic oxidation of benzyl alcohol to benzaldehyde and degradation of methyl orange (MO). The BiOCl HPs have featured high photocatalytic activity toward the selective aerobic oxidation of benzyl alcohol to benzaldehyde (735.7 μmol $gcat^{-1}$) at room temperature. The catalysts also exhibit remarkable photocatalytic activity toward the degradation of organic dyes.

Porous BiOCl hexagonal prisms were synthesized using a glucosamine hydrochloride as Cl^- resource (see ESI for details). As shown in Fig. 1, the powder X-ray diffraction (XRD) pattern can be easily indexed to tetragonal BiOCl crystallites, and the lattice parameters are in good agreement with the standard values (JCPDS No.73-2060). Fig. 2a and S1a,b show the low-magnification field-emission scanning electron microscope (FESEM) image of BiOCl materials. It can be clearly seen that

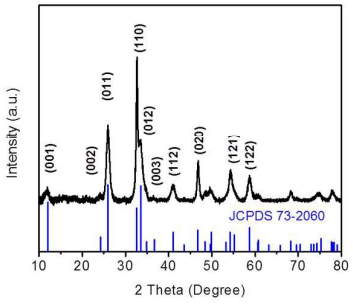

Fig. 1 XRD pattern of porous BiOCl HPs.

[a] Key Laboratory of Catalysis and Materials Science of the State Ethnic Affairs Commission & Ministry of Education, South-Central University for Nationalities, Wuhan, 430074, (China), E-mail: jchu@mail.scuec.edu.cn.
[b] Institute for Superconducting and Electronic Materials, School of Mechanical, Materials and Mechatronics Engineering, University of Wollongong, North Wollongong, New South Wales 2500, Australia.

* J. Hu is grateful for the financial support of Natural Science Foundation of Hubei Province (2013CFA089) and the Special Fund for Basic Scientific Research of Central Colleges, South-Central University for Nationalities (CZZ11002).
Electronic Supplementary Information (ESI) available: [details of any supplementary information available should be included here]. See DOI: 10.1039/x0xx00000x

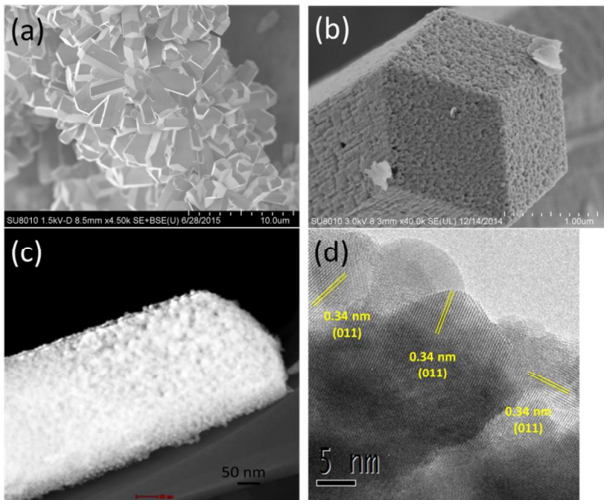

Fig. 2 Porous BiOCl HPs structural characterization: (a, b) FESEM images. (c, d) TEM images.

the as-prepared BiOCl is completely composed of a novel hexagonal prism with a rim of 1 µm and a length up to 6 µm. The magnified FESEM images (as shown in Fig. 2b and S2a,b) reveal that these BiOCl HPs are randomly assembled by numerous nanoparticles. Unlike the conventional hexagonal prisms having smooth surface[22-24], the surface of our prisms has many pores. High-resolution scanning electron microscope (HRSEM) image (Fig. S2c) records at the tip of an individual structure highlight the porous structure of the building blocks. More specifically, the primary BiOCl nanocrystals are self-assembled, consequently resulting in the formation of porous BiOCl HPs[25,26]. Moreover, to confirm the chemical composition and elemental distribution, SEM energy-dispersive X-ray (SEM-EDX) elemental analysis has been conducted on the porous BiOCl HPs. The mapping images reveal that bismuth, chlorine and oxygen elements are homogeneously distributed through the entire area (Fig. S1c-f and S2c-f). Besides, the EDX line scans elucidate that the signal patterns of Bi, Cl and O are the same (Fig. S3). The porous hexagonal prisms structures are further elucidated by field-emission transmission electron microscopy (FETEM) (Fig. 2c and S4). The selected area electron diffraction (SAED) pattern of the BiOCl HPs (Fig. S4b) suggests that the products have a polycrystalline nature. Fig. 2d shows a representative high-resolution TEM (HRTEM) image of a single porous BiOCl HPs. The well-resolved fringe spacing is about 0.34 nm, corresponding to the (011) crystal planes of tetragonal BiOCl. The high-angle annular dark-field (HAADF)-scanning STEM-EDX dot scan results clearly illustrate the presence of Bi, Cl and O again (Fig. S5). However, the atom ratio of Bi to Cl can't be determined because one peak for Bi overlapped with the peak for Cl[11]. From the above SEM and TEM results, we also observe that the BiOCl HPs material possess porous structures caused by nanoparticles. And the sizes of pores are measured to be 10-40 nm.

Furthermore, the X-ray photoelectron spectroscopy (XPS) measurements confirm that the porous BiOCl HPs contain Bi, Cl and O elements (Fig. S6). The binding energies of Bi $4f_{7/2}$ and Bi $4f_{5/2}$ peaks are located at 159.3 and 164.7 eV, respectively, which confirms the Bi^{3+} state in BiOCl (Fig. S6b)[27]. The peaks with binding energies of 198.1 and 199.7 eV in the Cl 2p spectrum are attributed to the Cl^- in BiOCl (Fig. S6c)[8]. The O 1s core level spectrum (Fig. S6d) is fitted with the peak at 530.7 eV, belonging to O^{2-} from a Bi-O bond in BiOCl[2]. In addition, time-dependent and temperature-dependent SEM results (Fig. 3, see also Fig. S8-S11 and Fig. S14-S16) in conjunction with the corresponding XRD results (Fig. S7 and S13) have been studied detailed to address of the possible formation mechanism of porous BiOCl HPs. We can see clearly that, the hexagonal

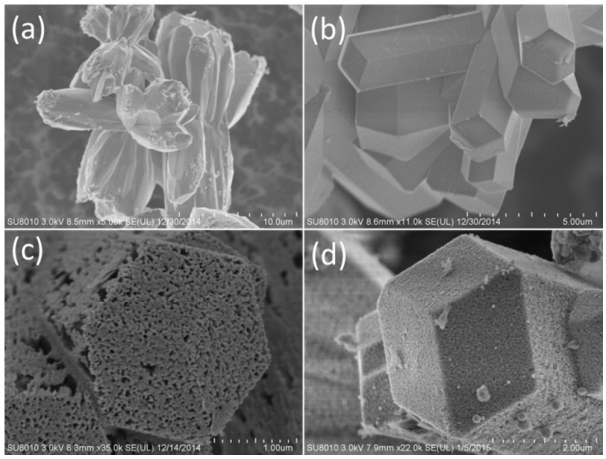

Fig. 3 (a-i) FESEM images of BiOCl HPs reacted for (a) 1 h, (b) 2 h, (c) 5 h, (d) 10 h.

structure BiOCl appears after 1 h reaction (Fig. 3a and S8) and grows to form geometrical hexagonal prism (Fig. 3b and S9). After being treated for 5 h, the BiOCl nanoparticles further assemble around the hexagonal prism, accompany with the decomposition of glucosamine, thus resulting in a porous structures (Fig. 3c and S10). Subsequently, the porous hexagonal prism BiOCl with regular shape is formed (Fig. 3d and S11). In order to demonstrate the porous structures, we further study the BET nitrogen adsorption-desorption isotherms (as shown in Fig. 4a and S12). In all cases, these isotherms can be ascribed to type Ⅳ with a hysteresis loops observed in the range of (0.6-1.0) P/P_0, indicating the presence of mesoporous structures[28]. Pore sizes are estimated to be 30 nm. These results are in agreement with the previous SEM and TEM observations. Details on BET surface areas and pore volumes are shown in Table S1. The studies of the functional groups in this reaction are also employed to better understanding of the possible formation mechanism (Fig. S17). As shown in Fig. S17a,b, the appearance of the hydroxyl groups stretching vibration at 3420 cm^{-1} mainly originates

from free water. The band at 1620 cm^{-1} is ascribed to C=C vibration demonstrates aromatization of glucosamine[29]. And the bands in the range of 1000-1300 cm^{-1} include the C-OH stretching and OH bending vibrations, suggestive of the existence of residual hydroxy groups. For comparison, the FT-IR spectra of BiOCl HPs and glucosamine hydrochloride are also measured (Fig. S17c). The peaks located at 3300 and 2950 cm^{-1} are due to N-H and C-H stretching vibrations of $C_6H_{13}NO_5$·HCl. Two strong peaks at 529 and 1390 cm^{-1} of BiOCl HPs can be assigned to the typical asymmetrical and symmetrical stretching vibrations of Bi-O[30,31]. Furthermore, a peak at 1083 cm^{-1} is attributed to the Bi-Cl[32]. These results disclose that glucosamine hydrochloride is decomposed gradually to form a porous BiOCl HPs.

On the basis of the results and discussions, the whole process may be divided into three steps. The synthesis process for the porous BiOCl HPs is schematically illustrated in Fig. S18. During the synthesis process, a solution can be obtained when $Bi(NO_3)_3$ and $C_6H_{13}NO_5$•HCl are dissolved into CH_3OH. In the first step, the glucosamine molecules are easily to coordinate with Bi^{3+}, forming a hexagonal chelating coordination structures[23]. Then, Cl^- is adsorbed preferably on the well-aligned molecules surfaces. During step 2, under the solvothermal conditions, BiOCl nuclei form rapidly around glucosamine molecules. With the extending of reaction time or increasing reaction temperature, glucosamine is decomposed gradually, thus form a porous structure. The BiOCl hexagonal arrays are formed in a stepwise self-assembly process. In step 3, BiOCl nanoparticles further stack along one direction, consequently come into being hexagonal prism.

The UV-visible diffuse reflectance spectra of the BiOCl powder are measured to determine their light absorption characteristics (Fig. S19). It is clearly reveal that the samples all show a major absorption band between 375 nm and 450 nm, which indicate that these porous BiOCl HPs can efficiently absorb visible light. The photocatalytic selective oxidation of benzyl alcohols are carried out under simulated sunlight and visible light irradiation, respectively. In our experiment, we have only detected the peaks of benzyl alcohol and benzaldehyde (see in Fig. S20), which suggests a high chemoselectivity[33,34]. As shown in Fig. 4b, negligible amounts of benzaldehyde are detected without catalysts. Under simulated sunlight irradiation, the BiOCl HPs show different photocatalytic activities. Obviously, the porous BiOCl HPs (obtained at 5 h) exhibit a much higher photocatalytic activity (735.7 μmol $gcat^{-1}$ product, 8 h) than other catalysts. Traces of benzyl alcohol will be adsorbed on BiOCl HPs because of the interaction between benzyl alcohol and surface hydroxyl groups during reaction. We have found that the as-prepared porous BiOCl HPs at 5 h possess the largest specific surface area of 32.1 m^2/g (Table S1), which is beneficial to the adsorption of benzyl alcohol. The porous BiOCl HPs (obtained at 5 h) also show the excellent photocatalytic activity (197.8 μmol $gcat^{-1}$ product, 8 h) under visible light irradiation. Considering that the different porous BiOCl HPs exhibit different specific surface area, it is reasonable to conclude that the different photocatalytic activities may be attributed to these unique porous structure[35]. Further work is in progress to understand the mechanism of photocatalytic selective oxidation of benzyl alcohols. The photocatalytic performances of the porous BiOCl HPs are also evaluated using MO as the probe molecule under visible light and ultraviolet light irradiation, respectively. The photocatalytic degradation of dyes can be divided into direct semiconductor photoexcitation and indirect dye photosensitization[12]. Under visible light irradiation, MO can be excited and the dye photosensitization process also depends on the photocatalyst's surface. Fig. 4c shows that the BiOCl HPs photocatalysts exhibit excellent photocatalytic activities for the MO degradation. Among them, the as-prepared porous BiOCl HPs at 5 h exhibit the highest photocatalytic activity. Furthermore, Fig. S21 shows the linear relationship between $\ln(C_0/C)$ and irradiation time indicating

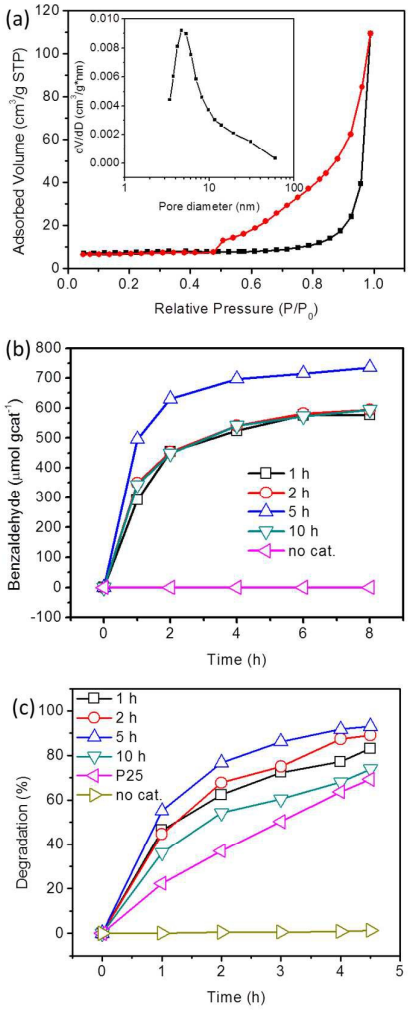

Fig. 4 Porous BiOCl HPs: (a) N_2 adsorption-desorption isotherms and pore size distributions (inset). (b) The photocatalytic oxidation activity of benzyl alcohol over different catalysts under simulated sunlight irradiation. (c) Comparative studies of MO degradation under visible light irradiation over different catalysts.

that the photocatalytic degradation of MO is a pseudo-first-order reaction. The apparent reaction rate constants have been listed in Table S2. The porous BiOCl HPs obtained at 5 h have the largest specific surface area, which may suggest that the photosensitization degradation process is strongly associated with the surface area[2]. MO is slightly self-degraded in the absence of photocatalyst and the presence of porous BiOCl HPs result in obvious degradation of MO (Fig. S22). The corresponding TOC changes in Fig. S23 proved that it is a mineralization process. The stability of the BiOCl HPs during photocatalytic reaction is further explored by repeat tests, XRD and SEM measurements (Fig S24-S26). These results revealed that the BiOCl HPs are stable during photocatalysis.

In conclusion, we have demonstrated a simple synthetic approach to prepare well-defined porous BiOCl HPs. The porous structure BiOCl exhibits a hexagonal prism morphology with a rim of 1 μm and a length up to 6 μm. These BiOCl HPs are assembled by numerous nanoparticles. They show strong absorption in the visible range. The BiOCl HPs have featured high photocatalytic activity and excellent selectivity toward the aerobic oxidation of benzyl alcohol to benzaldehyde under simulated sunlight and visible light irradiation, respectively. Meanwhile, they also have exhibited excellent photocatalytic activities for the MO degradation under visible light. The superior photocatalytic performances may attribute to unique structure.

Notes and references

1 H. F. Cheng, B. B. Huang and Y. Dai, *Nanoscale*, 2014, **6**, 2009-2026.
2 L. Y. Ding, R. J. Wei, H. Chen, J. C. Hu and J. L. Li, *Appl. Catal. B: Environ.*, 2015, **172-173**, 91-99.
3 L. L. Li, L. H. Ai, C. H. Zhang and J. Jiang, *Nanoscale*, 2014, **6**, 4627-4634.
4 J. Li, Y. Yu and L. Z. Zhang, *Nanoscale*, 2014, **6**, 8473-8488.
5 G. F. Li, F. Qin, R. M. Wang, S. Q. Xiao, H. Z. Sun and R. Chen, *J. Colloid Interface Sci.*, 2013, **409**, 43-51.
6 L. Y. Ding, C. Y. Zhang, Q. Q. Jiang, H. Chen, W. Sun and J. C. Hu, *Mater. Lett.*, 2015, **158**, 229-232.
7 H. Li, J. Shang, Z. H. Ai and L. Z. Zhang, *J. Am. Chem. Soc.*, 2015, **137**, 6393-6399.
8 Y. H. Wu, B. Yuan, M. R. Li, W. H. Zhang, Y. Liu and C. Li, *Chem. Sci.*, 2015, **6**, 1873-1878.
9 X. Xiao, C. Liu, R. Q. Hu, X. X. Zuo, J. M. Nan, L. S. Lia and L. S. Wang, *J. Mater. Chem.*, 2012, **22**, 22840-22843.
10 J. W. Wang and Y. D. Li, *Chem. Commun.*, 2003, **21**, 2320-2321.
11 H. Deng, J. W. Wang, Q. Peng, X. Wang and Y. D. Li, *Chem. Eur. J.*, 2005, **11**, 6519-6524.
12 J. Jiang, K. Zhao, X. Y. Xiao and L. Z. Zhang, *J. Am. Chem. Soc.*, 2012, **134**, 4473-4476.
13 M. L. Guan, C. Xiao, J. Zhang, S. J. Fan, R. An, Q. M. Cheng, J. F. Xie, M. Zhou, B. J. Ye and Y. Xie, *J. Am. Chem. Soc.*, 2013, **135**, 10411-10417.
14 H. P. Li, J. Y. Liu, X. F. Liang, W. G. Hou and X. T. Tao, *J. Mater. Chem. A*, 2014, **2**, 8926-8932.
15 J. Y. Xiong, G. Cheng, G. F. Li, F. Qin and R. Chen, *RSC Adv.*, 2011, **1**, 1542-1553.
16 F. Tian, Y. F. Zhang, G. F. Li, Y. L. Liu and R. Chen, *New J. Chem.*, 2015, **39**, 1274-1280.
17 X. F. Chang, S. B. Wang, Q. Qi, M. A. Gondal, S. G. Rashid, D. Y. Yang, M. A. Dastageer, K. Shen, Q. Y. Xu and P. Wang, *Appl. Catal. B: Environ.*, 2015, **176-177**, 201-211.
18 D. F. Sun, J. P. Li, Z. H. Feng, L. He, B. Zhao, T. Y. Wang, R. X. Li, S. Yin and T. Sato, *Catal. Commun.*, 2014, **51**, 1-4.
19 Y. Mi, L. Y. Wen, Z. J. Wang, D. W. Cao, Y. G. Fang and Y. Lei, *Appl. Catal. B: Environ.*, 2015, **176-177**, 331-337.
20 F. Tian, J. Y. Xiong, H. P. Zhao, Y. L. Liu, S. Q. Xiao and R. Chen, *CrystEngComm*, 2014, **16**, 4298-4305.
21 J. Y. Xiong, G. Cheng, F. Qin, R. M. Wang, H. Z. Sun and R. Chen, *Chem. Eng. J.*, 2013, **220**, 228-236.
22 Y. Hu, J. F. Chen, X. Xue, T. W. Li and Y. Xie, *Inorg. Chem.*, 2005, **44**, 7280-7282.
23 G. Z. Wang, L. Zhang, H. X. Dai, J. G. Deng, C. X. Liu, H. He and C. T. Au, *Inorg. Chem.*, 2008, **47**, 4015-4022; M. Ba¸czkowicz, D. Wo´jtowicz, J. W. Anderegg, C. H. Schilling and P. Tomasik, *Carbohyd. Polym.*, 2003, **52**, 263-268; A. Burkhardt and W. Plass, *Inorg. Chem. Commun.*, 2008, **11**, 303-306.
24 Y. R. Shi, Y. H. Wang, D. Wang, B. T. Liu, Y. H. Li and L. Wei, *Cryst. Growth Des.*, 2012, **12**, 1785-1791.
25 Y. Shang, Y. M. Shao, D. F. Zhang and L. Guo, *Angew. Chem. Int. Ed.*, 2014, **53**, 11514-11518.
26 B. Kong, J. Tang, C. Selomulya, W. Li, J. Wei, Y. Fang, Y. C. Wang, G. F. Zheng and D. Y. Zhao, *J. Am. Chem. Soc.*, 2014, **136**, 6822-6825.
27 Y. Ma, Y. L. Jia, Z. B. Jiao, M. Yang, Y. X. Qi and Y. P. Bi, *Chem. Commun.*, 2015, **51**, 6655-6658.
28 J. S. Xu and Y. J. Zhu, *ACS Appl. Mater. Interfaces*, 2012, **4**, 4752-4757.
29 J. Qi, K. Zhao, G. D. Li, Y. Gao, H. J. Zhao, R. B. Yu and Z. Y. Tang, *Nanoscale*, 2014, **6**, 4072-4077.
30 J. E. D. Davies, *J. Inorg. Nucl. Chem.*, 1973, **35**, 1531-1534.
31 L. Liu, J. Jiang, S. M. Jin, Z. M. Xia and M. T. Tang, *CrystEngComm*, 2011, **13**, 2529-2532.
32 J. M. Song, C. J. Mao, H. L. Niu, Y. H. Shen and S. Y. Zhang, *CrystEngComm*, 2010, **12**, 3875-3881.
33 A. Li, P. Zhang, X. X. Chang, W. T. Cai, T. Wang and J. L. Gong, *Small*, 2015, **11**, 1892-1899.
34 S. J. Liang, L. R. Wen, S. Lin, J. H. Bi, P. Y. Feng, X. Z. Fu and L. Wu, *Angew. Chem., Int. Ed.*, 2014, **53**, 2951-2955.
35 Z. F. Bian, T. Tachikawa, P. Zhang, M. Fujitsuka and T. Majima, *Nat. Commun.*, 2014, **5**, 3038-3046.

